remote sensing

MDPI

Article

A Three-Step Method for Determining Unhealthy Time Period of GPS Satellite Orbit in Broadcast Ephemeris and Its Preliminary Applications for Precise Orbit Determination

Fei Ye [1,2,3], Yunbin Yuan [1,2,*], Baocheng Zhang [1,2], Bingfeng Tan [1,2] and Jikun Ou [1,2]

1 Institute of Geodesy and Geophysics, CAS, 340 Xudong Street, Wuhan 430077, China; feiye@whigg.ac.cn (F.Y.); b.zhang@asch.whigg.ac.cn (B.Z.); bingfengtan@whigg.ac.cn (B.T.); ojk@asch.whigg.ac.cn (J.O.)
2 State Key Laboratory of Geodesy and Earth's Dynamics, 340 Xudong Street, Wuhan 430077, China
3 College of Earth and Planetary Sciences, University of Chinese Academy of Sciences, A19 Yuquan Road, Beijing 100049, China
* Correspondence: yybgps@whigg.ac.cn; Tel.: +86-027-68881072

Received: 13 March 2019; Accepted: 6 May 2019; Published: 8 May 2019

Abstract: Abnormal information of satellite orbits inevitably appears in the broadcast ephemeris. Failure to obtain unhealthy information on GPS satellite orbits in precise orbit determination (POD) degrades GPS service performance. At present, the reliable unhealthy information published by the Center for Orbit Determination in Europe (CODE) is usually used, but it has at least one-day latency, and the current level of unhealthy information cannot fully meet the requirements of rapid and real-time geodetic applications, especially for non-IGS (International global navigation satellite systems (GNSS) Service) analysis centers and BeiDou navigation satellite system (BDS) users. Furthermore, the unhealthy orbit information detected by the traditional method, which is based on the synchronized pseudo-range residuals and regional observation network, cannot meet the requirement of setting separate sub-arcs in POD. In view of these problems, we propose a three-step method for determining unhealthy time periods of GPS satellite orbit in broadcast ephemeris during POD to provide reliable unhealthy information in near-real time. This method is a single-epoch solution, and it can detect unhealthy time periods in each sampling of observation in theory. It was subsequently used to detect unhealthy time periods for satellites G09 and G01 based on the 111 globally distributed tracking stations in the IGS. The performance of the new method was evaluated using cross-validation. Based on the test results, it detected an orbital leap for G09 in the broadcast ephemeris from 09:59:42 to 14:00:42 on 25 August 2017. Compared to the traditional method, the unhealthy start time using the three-step method was in better agreement with the information provided by CODE's satellite crux files. G01 did not appear to have an orbital leap on the specified date, but it was misjudged by the traditional method. Furthermore, compared to the traditional method, the three-step method can perform unhealthy time period detection for a satellite all day long. In addition, precise orbit determination for unhealthy satellites is realized successfully with the unhealthy orbit arc information identified in this study. Compared to the CODE orbit, the root mean square and standard deviation of the new method for G09 are less than 2 cm, and the three-step method shows an improvement in accuracy compared with the traditional method. From the above results, it can be seen that this study can provide a feasible approach to meet the real-time unhealthy time period detection requirements of a satellite orbit in a broadcast ephemeris during POD. Furthermore, compared to waiting for updates of CODE's satellite crux files or for accumulating delayed observation data, it has the potential to provide additional information in the process of generating ultra-rapid/real-time orbits.

Keywords: three-step method; unhealthy orbit detection; precise orbit determination (POD); broadcast ephemeris; single-epoch solution

1. Introduction

Satellite orbit determination is critical for the maintenance of global navigation satellite systems (GNSS) service. Factors that affect its accuracy and stability have been widely researched (e.g., [1–6]). In addition, high-precision and reliable orbit products are expected by GNSS users for various geodetic and atmospheric applications (e.g., [7–10]). Guo et al. assessed the orbit accuracy of IGS multi-GNSS experiment (MGEX) [11]. Kazmierski et al. also assessed multi-GNSS real-time orbit accuracy [12]. On the other hand, a priori satellite orbits, as well as the partial derivatives of orbit positions, are the basis of precise orbit determination (POD). The broadcast ephemeris is often used to create the a priori orbit [13], and the Bancroft algorithm is usually used to estimate the a priori orbit of newly launched satellites [14,15]. Unfortunately, although there are many corrections and checks in the process of generating and receiving a broadcasting ephemeris, it may still contain inaccurate information [16,17]. Besides, Earth's non-uniform gravity, other perceptual factors, and other issues could lead to an offset in the satellite location. Therefore, satellite maneuvers are needed to keep the satellite in the nominal or temporary orbital position. Broadcast ephemerides, as one of the sources of predicted orbits, will inevitably be affected by the lack of timely updates. In the case of a maneuver, separate sub-arcs are set up for the maneuvering satellite in a multi-day solution [18]. In real-time applications, we generally use predicted orbits, called broadcast ephemerides and ultra-rapid products. It is risky to use the maneuvered satellite, which is undetected [19]. It is particularly important to detect unhealthy time periods of satellite orbits, especially when the broadcast ephemeris is used as the initial orbit source in precise orbit determination.

Satellite laser ranging can monitor Geostationary Orbit (GEO) satellite maneuvers. However, a corresponding laser gauging system for GNSS satellites is needed [20]. Similarly, based on C-Band pseudo-ranges, the C-Band transfer method can be used to detect satellite maneuvers. However, for mid-earth orbit (MEO) and inclined geosynchronous orbit (IGSO) satellites, it is necessary to build a large number of C-Band stations to achieve monitoring all day long [21]. Furthermore, satellite maneuvers can also be detected using radar data, which provide the state of motion for space targets, but this method is difficult to implement for GNSS satellites [22]. Satellite maneuvers can be detected in the post mode using the broadcast ephemeris. However, the method cannot meet real-time requirements in theory and practice; additionally, it cannot determine the specific start maneuver epoch, and the time resolution is low [23]. Liu et al. developed a method to perform real-time anomaly detection of BeiDou navigation satellite system (BDS) broadcast ephemeris, but this method only analyzed the abnormal parameters of a broadcast ephemeris [24]. Huang et al. proposed methods to detect BDS satellite orbital maneuvers in real-time mode using a single BDS receiver, and they can be used to improve PNT services. Except for POD, these methods will be affected by the abnormal clock offset, and the time period detected by these methods cannot be defined as the real maneuvering time period of satellites [25,26]. Therefore, these methods cannot be fully applied to GNSS satellite POD when the broadcasting ephemeris is used as the initial orbit source.

The global observation data and broadcast ephemeris are provided by International GNSS Service (IGS), IGS multi-GNSS experiment, and International GNSS monitoring and assessment system. These observation data can be fully used to monitor satellite orbit of broadcast ephemeris all day long. Furthermore, the IGS has been developing the capability for real-time data streaming from the ground station network for some years [27], and the condition that unhealthy time periods are detected all day long in real-time for GPS satellite orbit by the real-time data is also gradually maturing. Currently, the Center for Orbit Determination in Europe (CODE, http://www.aiub.unibe.ch/download/BSWUSER52/GEN/SAT_yyyy.CRX, where yyyy is the four digit year), U.S. Coast Guard Navigation

Center (NAVCEN, https://www.navcen.uscg.gov/), and the broadcast ephemeris publish this type of information about satellites of broadcast ephemerides, but there is at least one day latency for CODE, and the maneuver detection algorithm of CODE is only suitable for processing in post mode [28,29]. Furthermore, the satellite state information of NAVCEN and the health flag for the broadcast ephemeris decrease observation utilization of unhealthy satellites. This information does not distinguish between satellite maneuvers and other anomalies as well. Furthermore, there are times when non-IGS analysis centers are not allowed access to the website of NAVCEN, and the information about BDS has not yet been published on similar websites in advance. In [30], the synchronized pseudo-range residuals were used as criteria to define the unhealthy time period of satellite orbits in broadcast ephemerides. Considering the innovative contributions of Tsai in [30], it is very necessary to consider it as the traditional method [30,31]. However, the traditional detection algorithm is only valid for the regional observation network. In this regional observation network, it is impossible to observe all satellites at the same time, and it is impossible to observe the same satellite all day long. Therefore, the traditional detection algorithm cannot detect unhealthy time periods all day long for satellite orbits. In addition, theoretically, it is susceptible to satellite maneuvers and abnormal values when eliminating the clock offset. Although the reliability of unhealthy time period detected by this method does not affect the performance of the wide area augmentation system (WAAS), it cannot meet the requirements of POD. In summary, the current state of satellite information cannot fully meet the requirements for rapid and real-time geodetic applications. Therefore, it is important to provide a feasible approach to perform reliably unhealthy orbit arc detection of broadcast ephemerides all day long in real-time during POD.

Based on the described limitations and requirements, in order to explore the possibility of obtaining a reliable single-epoch solution for unhealthy time period detection of the satellite orbit in a broadcast ephemeris during POD, we propose a three-step method using GPS observation data to detect unhealthy time periods of satellite orbits. The three-step method is described in Section 2. Evaluations of our new method against the traditional method are given in Sections 3 and 4. A conclusion is given in Section 5.

2. Materials and Methods

To eliminate the first-order ionosphere delay, the ionospheric-free (IF) linear combination is commonly used to express the GPS observation equation. In addition, to reduce the impact of multipath and noise, the IF carrier-smoothed pseudo-range equation for a receiver with dual-frequency signal capture is given as follows [32]:

$$P^s_{r,IF}(t) = \rho + Trop_r + \varepsilon_{P^s_{r,IF}},\ \sigma^2_{P^s_{r,IF}} \tag{1}$$

where t is the observation time of satellite orbit detection and $P^s_{r,IF}$ is the IF carrier-smoothed pseudo-range observation. Subscripts r and s represent the receiver and PRN of the satellite, respectively. ρ is the geometric distance between the receiver and satellite phase center, including clock offset, $Trop_r$ is the tropospheric delay, $\sigma^2_{P^s_{r,IF}}$ (elevation-dependent) is the variance of P [33], and ε is the noise.

In this paper, the receiver position was known, and the tropospheric delay was corrected by the model together with parameter estimation. Moreover, the satellite position and satellite clock offsets were initialized by the broadcast ephemeris. Then, the equation obtained after linearizing Equation (1) is

$$\Delta\rho^s_{r,IF}(\mathrm{t}) = \mu^s_r \Delta \mathrm{s} + \mathrm{c}dt_r - cdt^s + \varepsilon_{\Delta\rho^s_{r,IF}} \tag{2}$$

where $\Delta\rho^s_{r,IF}$ represents the pseudo-range residuals; μ^s_r is the unit line of sight vector from the receiver to the satellite; Δs are the ephemeris errors in radial dr, along-track da, and cross-track dc directions; and dt_r and dt^s are the receiver and satellite clock offsets with reference to the system time, respectively. c is the speed of light in a vacuum.

According to Equations (1) and (2), the pseudo-range residuals of different satellites are coupled by the receiver clock offsets. However, these receiver clock offset offsets contribute little in determining the unhealthy time period of the GPS satellite orbit. In this paper, these nuisance parameters were removed with the first two steps in the three-step method. The following sections describe the three-step method in detail.

2.1. The First Step: Calculating the Datum Clock Offset

Time is relative. Therefore, to eliminate receiver clock offsets, it was necessary to choose a datum clock [29,30]. To provide a stable datum, we selected a reference station clock equipped with an atomic clock. This reference station was called the datum station [34]. The datum clock offset was calculated as follows.

According to the accuracies of the satellite position and clock offsets for broadcast ephemerides [35], compared to the magnitude of satellite maneuvers and outliers, the accuracies of the satellite position and clock offsets were sufficient to meet the requirements for detecting unhealthy time period of GPS satellite orbit. For satellite abnormalities (e.g., orbit and clock offset outliers), we used the robust method to overcome their influences in estimating the datum clock offset [36]. Equation (2) can be rewritten as follows:

$$\Delta\rho^s_{m,IF}(t) = cdt_m + \varepsilon,\ \sigma^2_{\Delta\rho^s_{m,IF}} \tag{3}$$

where m stands for the receiver of the datum station, $\sigma^2_{\Delta\rho^s_{m,IF}} = \sigma^2_{P^s_{m,IF}} = 1/cos^2(z^s_m)$, and z is the zenith angle.

For all satellites observed by the datum station, the datum clock offsets can be estimated along with their variances using the robust method. The calculation procedures are described as follows.

1. The median of $\Delta\rho^s_{m,IF}$ is calculated as:

$$\overset{med}{\Delta\rho_m}(t) = median\left\{\Delta\rho^s_{m,IF}(t)\right\}, \tag{4}$$

   where $s = 1, 2, \ldots, N$, N is the number of satellites observed at the datum station, and the symbol $median\{.\}$ indicates the median calculated for this sequence $\Delta\rho^s_{m,IF}(t)$.

2. The initial residuals v_s are calculated as:

$$v_s = \Delta\rho^s_{m,IF}(t) - \overset{med}{\Delta\rho_m}(t). \tag{5}$$

3. The robust variance factor σ_0 is calculated as [36]:

$$\sigma_0 = median\{|v_s|\}/0.6745. \tag{6}$$

4. The robust weights $\widetilde{P}_s$ are calculated as [36]:

$$\widetilde{P}_s = \begin{cases} 0, |v_s| > c_0\sigma_0 \\ \frac{1}{\sigma^2_{\Delta\rho^s_{m,IF}}}, |v_s| \le c_0\sigma_0 \end{cases}, \tag{7}$$

   where we selected $c_0 = 3$ in this work.

5. Calculate the datum clock offset:

$$cdt_m = \left(\sum\nolimits_{s=1}^{s=N}(\widetilde{P}_s\Delta\rho^s_{m,IF})\right)/\left(\sum\nolimits_{s=1}^{s=N}\widetilde{P}_s\right). \tag{8}$$

After the datum clock offset is calculated, the other reference receiver offsets can be calculated using the second step.

2.2. The Second Step: Removing Receiver Clock Offsets of Other Reference Stations

Once the datum clock offset is calculated, the difference between the receiver clock offset of R^{th} reference station and datum clock offset can be used to estimate the reference receiver offsets of other reference stations. From Equation (2), we can have the following equation:

$$\begin{aligned} \Delta^s_{R,m}(t) &= \Delta\rho^s_{R,IF}(t) - \Delta\rho^s_{m,IF}(t) \\ &= \left(\mu^s_R \Delta \mathrm{s} + \mathrm{cd}t_R - cdt^s + \varepsilon_{\mathrm{R},P_{IF}}\right) - \left(\mu^s_m \Delta \mathrm{s} + \mathrm{cd}t_m - cdt^s + \varepsilon_{\mathrm{m},P_{IF}}\right) \\ &= \left(\mu^s_R - \mu^s_m\right)\Delta \mathrm{s} + \Delta \mathrm{cd}t_{R,m} + \varepsilon_{R,m},\ \sigma^2_{\Delta^s_{R,m}} \end{aligned} \tag{9}$$

where $\Delta^s_{R,m}$ is the difference value of the pseudo-range residuals between the datum receiver m and receiver R of other reference station, and $R = 1, 2, \ldots J$.

In this study, we divided the selected IGS global reference network into six smaller regional networks; in addition to the datum station, we assumed that J is the number of reference stations in each regional network, while the number of reference stations in each regional network can vary. In fact, the requirement of real-time detection can be met, as long as we can ensure that the uptime of the proposed method is less than one second. Therefore, considering the size of each regional network and the quality of the broadcast ephemeris, Equation (9) can be rewritten as follows:

$$\Delta^s_{R,m}(t) = \Delta cdt_{R,m} + \varepsilon_{R,m} \tag{10}$$

$$\sigma^2_{\Delta^s_{R,m}} = \sigma^2_{\Delta\rho^s_{R,IF}} + \sigma^2_{\Delta\rho^s_{m,IF}}. \tag{11}$$

Based on Equations (10) and (11), the calculation procedures of $\Delta cdt_{R,m}$ are described as follows:

1. The median of $\Delta^s_{R,m}$ is calculated as:

$$\overset{med}{\Delta}_{R,m}(t) = median\left\{\Delta^s_{R,m}(t)\right\}. \tag{12}$$

2. The initial residuals v^s_Δ are calculated as:

$$v^s_\Delta = \Delta^s_{R,m}(t) - \overset{med}{\Delta}_{R,m}(t). \tag{13}$$

3. The robust variance factor $\sigma_{v_{\Delta 0}}$ is calculated as:

$$\sigma_{v_{\Delta 0}} = median\left\{\left|v^s_\Delta\right|\right\}/0.6745. \tag{14}$$

4. The robust weights $\widetilde{P^s_\Delta}$ are calculated as:

$$\widetilde{P^s_\Delta} = \begin{cases} 0, \left|v^s_\Delta\right| > c_0\sigma_{v_{\Delta 0}} \\ \frac{1}{\sigma^2_{\Delta^s_{r,m}}}, \left|v^s_\Delta\right| \le c_0\sigma_{v_{\Delta 0}} \end{cases}. \tag{15}$$

5. Calculate the reference receiver clock offset:

$$\Delta cdt_{R,m} = \left(\sum\nolimits_{s=1}^{s=N}\left(\widetilde{P^s_\Delta}\Delta^s_{R,m}\right)\right)/\left(\sum\nolimits_{s=1}^{s=N}\left(\widetilde{P^s_\Delta}\right)\right). \tag{16}$$

Because cdt_m and $\Delta cdt_{R,m}$ are known, the pseudo-range residuals of the R^{th} reference receiver can be expressed using Equation (17), while Equation (9) can be expressed as Equation (18):

$$\mathrm{d}\rho^s_{R,IF}(t) = \Delta\rho^s_{R,IF}(t) - cdt_R = \Delta\rho^s_{R,IF}(t) - \Delta cdt_{R,m} - cdt_m = \mu^s_R \Delta \mathrm{s} - cdt^s + \varepsilon_{\mathrm{R},P_{IF}} \tag{17}$$

$$d\Delta^s_{R,m}(t) = \Delta^s_{R,m}(t) - \Delta c dt_{R,m} = \left(\mu^s_R - \mu^s_m\right)\Delta s + \varepsilon_{R,m}. \tag{18}$$

6. Calculate $d\rho^s_{R,IF}(t)$ and $d\Delta^s_{R,m}(t)$ according to Equations (17) and (18).

After $d\rho^s_{R,IF}(t)$ and $d\Delta^s_{R,m}(t)$ are calculated, the reference receiver offsets are removed from them. Then, the two threads can be used to detect unhealthy time periods of the satellite orbit in the third step.

2.3. The Third Step: Detecting Unhealthy GPS Satellite Orbit Arc in Broadcast Ephemeris

Both $d\rho^s_{R,IF}(t)$ and $d\Delta^s_{R,m}(t)$ contain the effects of the ephemeris error Δs. Hence, they can complement each other. For reliability, stability, and accuracy, two threads should be used during detection of unhealthy time periods of the satellite orbit: One variable per thread. It is assumed that $s1$ is the PRN of the satellite to be detected.

2.3.1. Thread One

As $s1$ can be observed by some reference receivers in the regional network, the sequence $d\rho^s_{R,IF}(t)$ will be the final pseudo-range residual, which eliminates the receiver clock offset. The median $\overset{med}{\Delta\rho_{s1}}(t)$ is defined as the variable to be detected, and it is also defined as the synchronized pseudo-range residual.

$$\overset{med}{\Delta\rho_{s1}}(t) = median\left\{d\rho^{s1}_{R,IF}(t)\right\} \tag{19}$$

Once the object to be detected has been introduced, the strategy for detecting the unhealthy orbit arc is as follows:

1. The median of $d\rho^s_{R,IF}$ is calculated as:

$$\overset{med}{d\rho_{IF}}(t) = median\left\{d\rho^{s=1\ldots N}_{R=1\ldots J,IF}(t)\right\}. \tag{20}$$

2. The initial residuals (V^s_R and ΔV^{s1}) are calculated as:

$$\begin{cases} V^s_R = d\rho^{s=1\ldots N}_{R=1\ldots J,IF}(t) - \overset{med}{d\rho_{IF}}(t) \\ \Delta V^{s1} = \overset{med}{\Delta\rho_{s1}}(t) - \overset{med}{d\rho_{IF}}(t) \end{cases}. \tag{21}$$

3. The initial robust variance factor $\sigma_{V^s_R}$ is calculated as:

$$\sigma_{V^s_R} = median\left\{\left|V^s_R\right|\right\}/0.6745. \tag{22}$$

4. The robust factors $\alpha_{V^s_R}$ and their equivalent weights $\widetilde{P_{V^s_R}}$ are calculated as:

$$\alpha_{V^s_R} = \begin{cases} 0, \left|V^s_R\right| > c_0\sigma_{V^s_R} \\ 1, \left|V^s_R\right| \le c_0\sigma_{V^s_R} \end{cases} \tag{23}$$

$$\widetilde{P_{V^s_R}} = \alpha_{V^s_R}\frac{1}{\sigma^2_{\Delta\rho^s_{R,IF}}}. \tag{24}$$

5. The robust variance factor $\sigma_{\overset{med}{\Delta\rho_{s1}}(t)}$ is calculated as:

$$\sigma_{\overset{med}{\Delta\rho_{s1}}(t)} = \left(\sum\nolimits_{s=1.R=1}^{s=N,R=J}\left(V^s_R\widetilde{P_{V^s_R}}V^s_R\right)\right)/\left(\sum\nolimits_{s=1.R=1}^{s=N,R=J}\left(\alpha_{V^s_R}\right) - 1\right). \tag{25}$$

6. The detection conditions are provided as follows:

$$s1(t) = \begin{cases} Unusable \quad , \quad \left|\Delta V^{s1}\right| > c_0 \sigma_{\substack{med \\ \Delta\rho_{s1}(t)}} & (a) \\ Usable \quad , \quad \left|\Delta V^{s1}\right| \le c_0 \sigma_{\substack{med \\ \Delta\rho_{s1}(t)}} & (b) \end{cases}. \tag{26}$$

Based on the above steps, we can get the first judgment, and the second judgment will be introduced in Thread two.

2.3.2. Thread Two

Because $\Delta s1$ can reflect the offset between the predicted orbit and estimated orbit, and considering the predicted orbit accuracy, we set the offset threshold *Threshold*1 to 10 m [35]. Alternatively, we can calculate the offset threshold *Threshold*2 as shown in step 3 below. The calculation procedures are described as follows:

1. Calculate $\Delta s1\begin{pmatrix} dr & da & dc \end{pmatrix}$ according to Equation (18).
2. Calculate the three-dimensional error d^{s1}_{error}.

$$d^{s1}_{error}(t) = \sqrt{\begin{pmatrix} (dr)^2 & + & (da)^2 & + & (dc)^2 \end{pmatrix}} \tag{27}$$

3. If the consecutive number of calculated epochs in which the satellite orbit of the broadcast ephemeris maintained health status exceeds 10, a sequence can be obtained from Equation (28). The offset threshold *Threshold*2 can be calculated from Equation (29).

$$D^{s1} = \begin{pmatrix} d^{s1}_{error}(t-1) & d^{s1}_{error}(t-2) & \dots & d^{s1}_{error}(t-10) \end{pmatrix} \tag{28}$$

$$Threshold2 = c_0\Big(median\Big\{D^{s1}\Big\}/0.6745\Big) \tag{29}$$

4. The detection conditions are provided as follows:

$$s1(t) = \begin{cases} Unusable, & d^{s1}_{error}(t) > Threshold1 \quad or \quad d^{s1}_{error}(t) > Threshold2 & (a) \\ Usable, & d^{s1}_{error}(t) \le Threshold1 \quad and \quad d^{s1}_{error}(t) \le Threshold2 & (b) \end{cases} \tag{30}$$

We can get the second judgment based on Thread two. From now on, we use the above two judgment conditions to make the following comprehensive judgment.

2.3.3. Comprehensive Evaluation

Based on the results of above two threads, we can summarize that:

1. If both Equations (26a) and (30a) are satisfied at the same time within k_0 (in this draft, $k_0 = 5$) consecutive epochs, it can be assumed that there is an orbit leap in satellite $s1$ of broadcast ephemeris at time t, and a separate sub-arc will be set up at the begin-time t of the unhealthy time period when the broadcast ephemeris is used to create the a priori orbit during POD.
2. If either one of the Equations (26a) or (30a) is satisfied, it can be concluded that there is an orbital anomaly in satellite $s1$ of broadcast ephemeris at time t, and the observation data will be deleted at time t when the broadcast ephemeris is used to create a priori orbit during POD.
3. In all other cases, satellite $s1$ is usable at time t. When the satellite orbit of the broadcast ephemeris stays leaped or has an anomalous status before the time t, if this condition is met in this time t, then the unhealthy time period ends in this time t, and this time t is the unhealthy end-time.

From the above comprehensive evaluation, the unhealthy time period of the satellite orbit of the broadcast ephemeris can be obtained. Meanwhile, the unhealthy time period detection is also implemented simultaneously in multiple regional networks with multi-threads; if a leap or anomaly occurs in any satellite orbit in any regional networks, then this satellite orbit of broadcast ephemeris is considered to have a leap or anomaly. Therefore, this method allows unhealthy time period detection for a satellite all day long by comprehensive evaluation.

So far, the three-step method has been introduced, and in Sections 3 and 4, the proposed method is validated and analyzed using actual datasets.

3. Preliminary Analysis Results

To evaluate the performance of the described three-step method, we processed observations from 111 globally distributed stations shown in Figure 1. As shown in Figure 1, the different colors represent different regional networks and the five-pointed stars represent datum stations in each regional network. Table 1 also shows the number of stations per regional network and the datum station of each regional network. In fact, this number of stations per regional network can ensure that the uptime of the proposed method is much less than one second. GPS data were obtained from IGS CDDIS (crustal dynamics data information system). To have a comprehensive evaluation of the proposed method's performance, we used cross-validation; we compared results from the three-step method with information in CODE's satellite crux files, information from NAVCEN, and health flags from the broadcast ephemerides. Additionally, the proposed method was also compared with the traditional method. Considering the innovative contributions of Tsai in [30] and the convenience of comparison, the pseudo-range residuals processing method that does not use robust method in the three-step method was considered as the traditional method. In fact, the traditional method does not have the processing function of multiple threads.

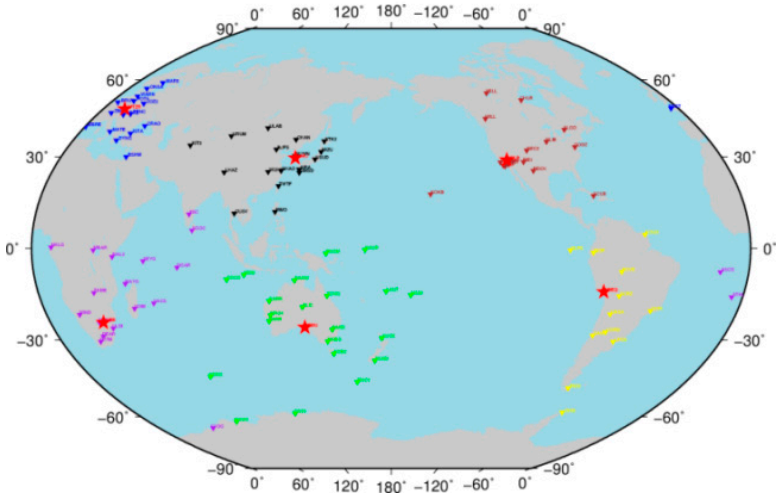

Figure 1. Distribution of global stations used for unhealthy orbit arc detection.

Table 1. Number of stations in selected regional network and the name of the datum station used in each regional network.

Regional Network	Number of Stations	Name of the Datum Station
1	19	GOL2
2	13	AREQ
3	17	WTZR
4	22	CEDU
5	18	DAEJ
6	22	HARB

For the validation, we selected and analyzed two-day data when there was a possibility that there could be an unhealthy time period of the satellite in the broadcast ephemeris: 25 August and 14 September 2017. The two-day data were separated for use in the case studies, and case 3 analyzed the impact of the unhealthy time period information detected using the first two case studies on POD. The details of the case studies are as follows.

Case 1: Satellite G09 ($s = 9$) testing on 25 August 2017 (the different colors mean the results from the different regional networks, and colors are consistent with colors of regional networks in Figure 1). Figures 2 and 3 show the proposed method's synchronized pseudo-range residuals and 3D error, respectively. Figure 4 shows the synchronized pseudo-range residuals using the traditional method. Table 2 summarizes the G09 status collected from the four validations and traditional methods.

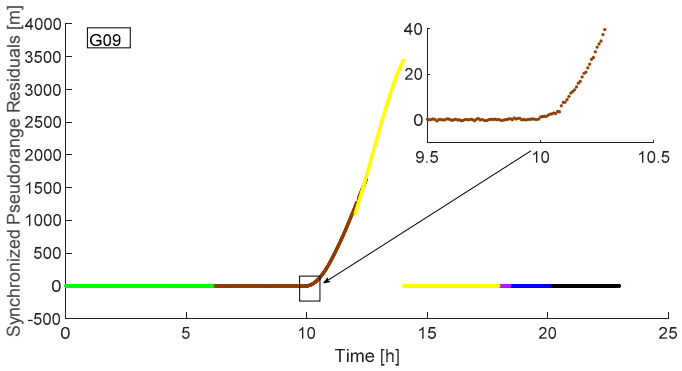

Figure 2. Synchronized pseudo-range residuals for satellite G09 using the three-step method.

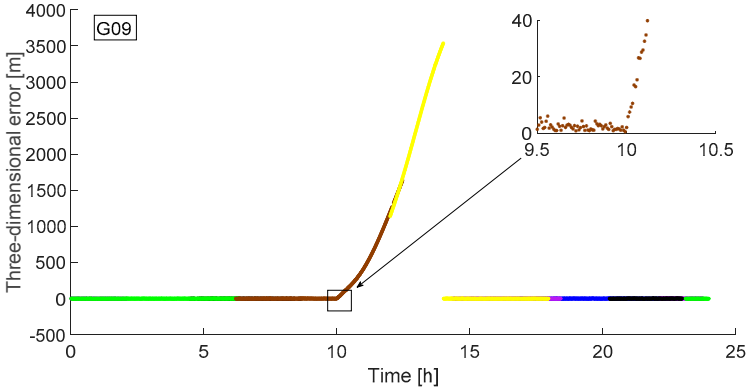

Figure 3. 3D error for satellite G09 using the three-step method.

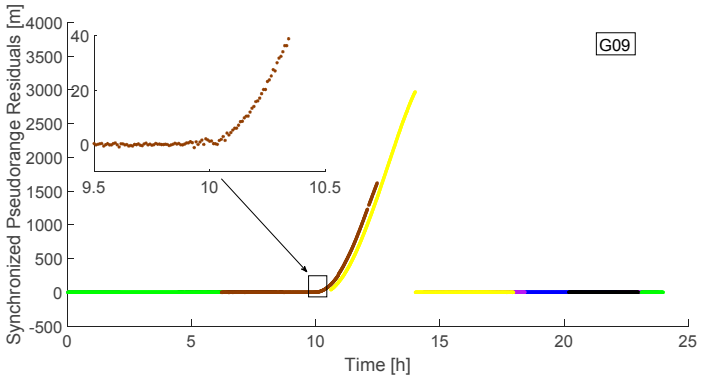

Figure 4. Synchronized pseudo-range residuals for satellite G09 using the traditional method.

Table 2. Validation results for satellite G09 of broadcast ephemeris for 25 August 2017.

PRN(G09): August 25, 2017		Unusable Start Time (UTC)	Unusable Stop Time (UTC)	Unhealthy Time Period (UTC)
Three-step Method	Thread one	09:59:42	14:00:42	09:59:42–14:00:42 (there is an orbit leap)
	Thread two	09:59:42	14:00:42	
	Comprehensive evaluation	09:59:42	14:00:42	
CODE's satellite crux files				09:59:28–(maneuver)
Information from NAVCEN		08:47:00	13:58:00	08:47:00–13:58:00
Health Flag from the Broadcast Ephemeris		09:59:26	15:57:02	09:59:26–15:57:02
Traditional Method		10:05:12	14:00:42	10:05:12–14:00:42 (there is an orbit leap)

As seen in Figures 2–4 and Table 2, the three-step method detected that the unhealthy time period was 09:59:42–14:00:42 for G09 of the broadcast ephemeris, and there was an orbit leap from 09:59:42 to 14:00:42; the CODE's satellite crux files showed that there was a maneuver for G09 at 09:59:28; the information from NAVCEN displayed that the unhealthy time period was 08:47:00–13:58:00 for G09 of the broadcast ephemeris; the health flag from the broadcast ephemeris showed that the unhealthy time period was 09:59:26–15:57:02 for G09; besides, the traditional method detected that the unhealthy time period was 10:05:12–14:00:42 for G09 of the broadcast ephemeris, and there was an orbit leap from 10:05:12 to 14:00:42. In the process of the traditional method, the detected results were affected by orbit leap when removing the receiver clock offset. Therefore, compared to the begin time detected by the three-step method, the begin time detected by the traditional method had about a 6-minute delay.

Case 2: Satellite G01 ($s = 1$) testing on 14 September 2017 (the different colors mean the results from the different regional networks, and colors are consistent with colors of regional networks in Figure 1). Figures 5 and 6 show the proposed method's synchronized pseudo-range residuals and 3D error, respectively. Figure 7 displays the synchronized pseudo-range residuals from the traditional method and Figure 8 displays the available number of observations from G01. Table 3 summarizes the G01 status based on the four validation and traditional methods.

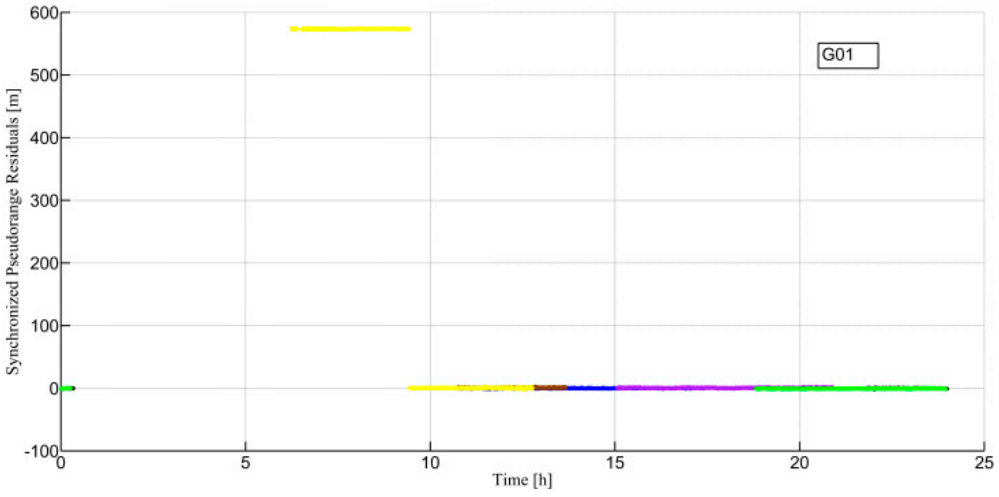

Figure 5. Synchronized pseudo-range residuals for satellite G01 using the three-step method.

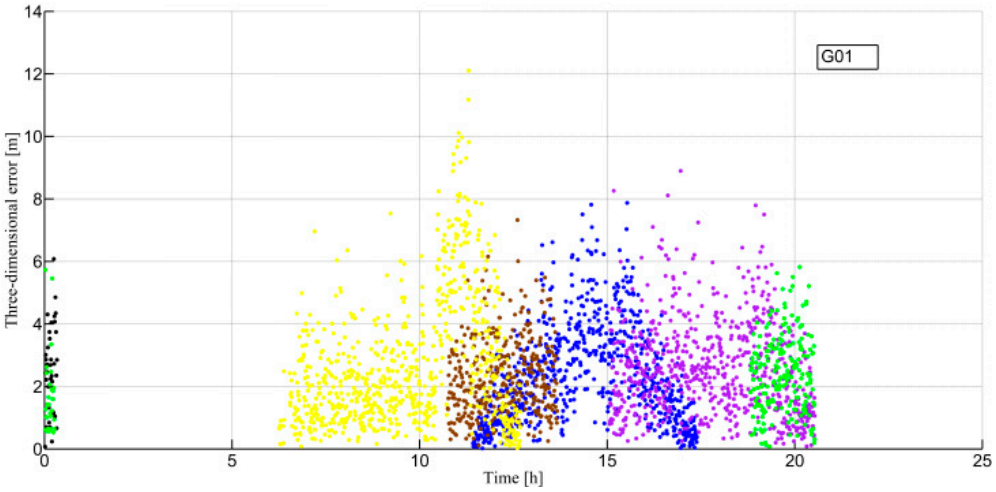

Figure 6. 3D error for satellite G01 using the three-step method.

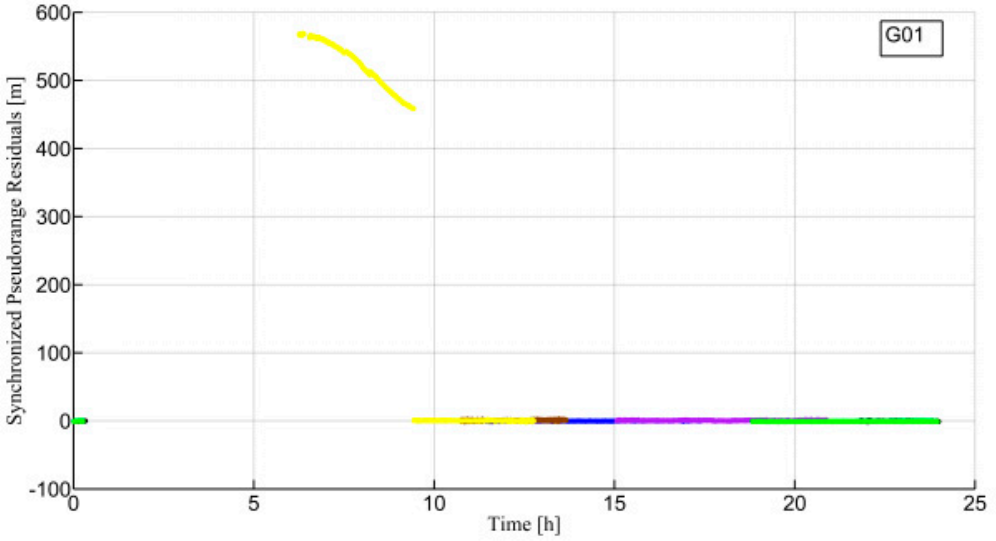

Figure 7. Synchronized pseudo-range residuals for satellite G01 using the traditional method.

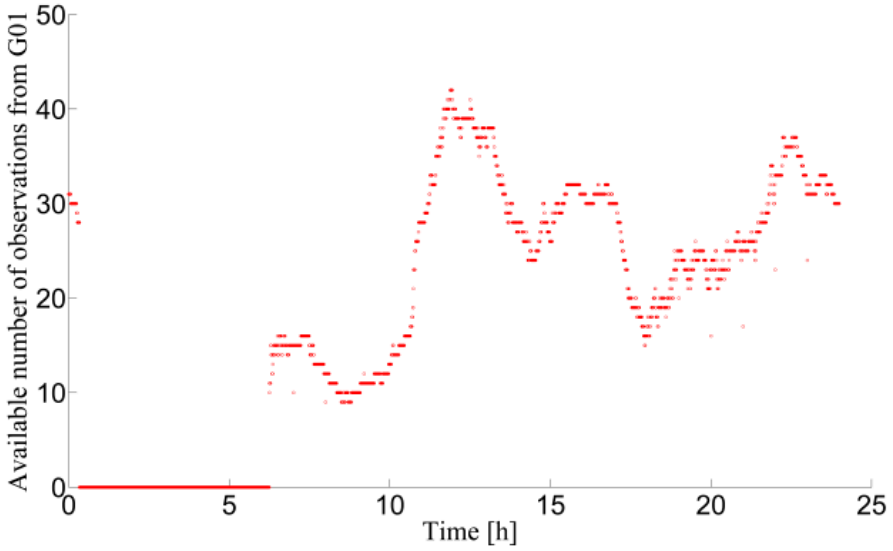

Figure 8. Available number of observations from satellite G01.

Table 3. Validation results for satellite G01 for 14 September 2017.

PRN(G01): September 14, 2017		Unusable Start Time (UTC)	Unusable Stop Time (UTC)	Unhealthy Time Period (UTC)
Three-step Method	Thread one	06:14:42	09:26:12	06:14:42–09:26:12
	Thread two			
	Comprehensive evaluation	06:14:42	09:26:12	
CODE's satellite crux files				
Information from NAVCEN		00:21:00	09:26:00	00:21:00–09:26:00
Health Flag from the Broadcast Ephemeris *		07:59:10	09:58:38	07:59:10–09:58:38
Traditional Method		06:14:42	09:26:12	06:14:42–09:26:12 (there is an orbit leap)

*: At UTC 01:59:42–07:59:10, the ephemeris data of G01 is missing.

As seen in Figures 5–7 and Table 3, the CODE's satellite crux files showed that there was not a maneuver for G01 on 14 September 2017; the information from NAVCEN displayed that the unhealthy time period was 00:21:00–09:26:00 for G01 of the broadcast ephemeris; the health flag from the broadcast ephemeris showed that the unhealthy time period was 07:59:10–09:58:38 for G01; furthermore, the three-step method and the traditional method detected that the unhealthy time periods were 06:14:42–09:26:12 for G01 of the broadcast ephemeris. Except for the traditional method, its results were affected by satellite clock offset, so this method misjudged that there was an orbit leap from 06:14:42 to 09:26:12 for G01 of the broadcast ephemeris.

Case 3: Overall testing of the impact of the unhealthy time period information on POD. In this case, we compared the computed orbit (termed the IGG/IGG01 orbit in this work) with the final orbit provided by CODE (termed the COD orbit in this work), for two scenarios: 1) IGG solution: The unhealthy time period information detected and used by the three-step method, 2) IGG01 solution: The unhealthy time period information detected and used by the traditional method.

The observation data from the IGS network for 25 August and 14 September 2017 were processed. Figure 9 shows the distribution of tracking stations used in this study. The key strategy for processing computed orbits using observation and force models are listed in Table 4.

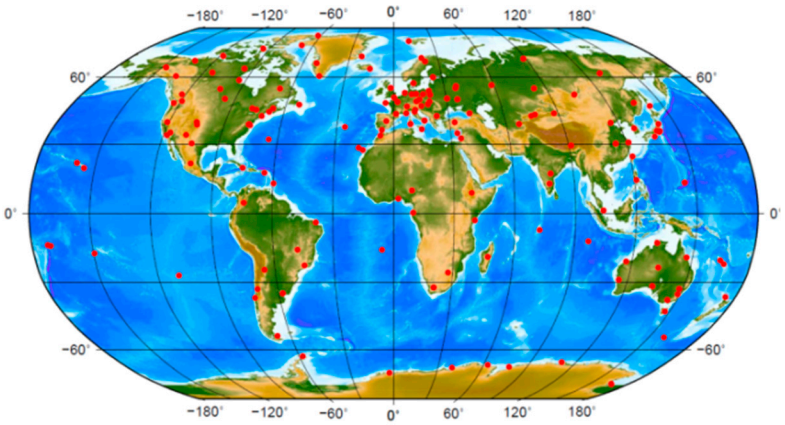

Figure 9. Distribution of tracking stations used for precise orbit determination (POD).

Table 4. Observation and force models.

Items	Description
Number of stations	~150
Processing mode	Middle day of 3-day arc
Processing scheme	Double-difference network processing (observable: phase double differences, ionosphere-free linear combination)
Elevation mask	5°; elevation-dependent weighting
Observation sampling period	30 s
Satellite/Receiver clock error	Double-difference
Ionosphere	Ionosphere-free linear combination
Tropospheric delay	GMF mapping function; ZHD: GPT model, ZWD is estimated every 2 h based on the piece-wise function [37,38]
A priori orbits	Broadcast ephemeris
A priori coordinates	Previous 3-day solution
Earth gravity	EGM2008 12 × 12
Solar radiation	ECOM 5-parameter model
Solid earth Tide and pole tide	IERS Conventions IERS2010
Ocean tide	FES2004
Nutation model	IAU2000
Satellite/Station phase center	Igs14.atx
N-body gravitation	Sun, Moon, and other planets (DE405)
Relativity effect	IERS Conventions IERS2010
Pseudo-stochastic pulses	12-h interval, at noon and at midnight of each calendar day
Satellite orbit leap	Set up SAT. with SVN = SVN + 50 [29]

Case 3 was divided into the following two tests:

1. The POD test based on data for 25 August 2017. Computed orbits (IGG solution, IGG orbits) were compared with the CODE orbits in the X, Y, and Z directions. The root mean square (RMS) and standard deviation (STD) values corresponding to the difference are displayed in Figures 10 and 11, respectively. The orbit differences between IGG01 solution (IGG01 orbits) and COD are shown in Figure 12. The statistical results for G09 are listed in Table 5.

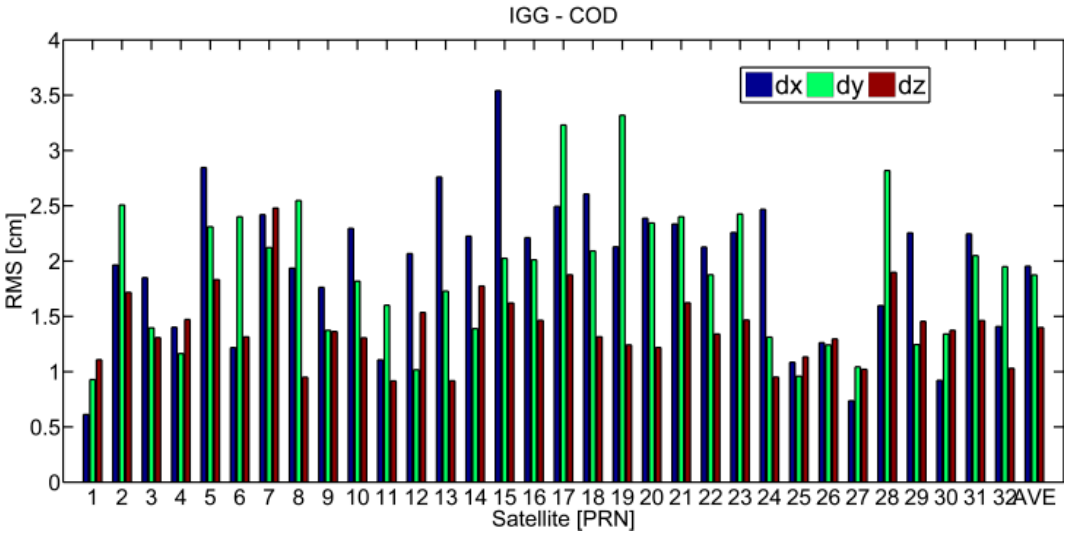

Figure 10. Root mean square (RMS) values using the three-step method for 25 August 2017.

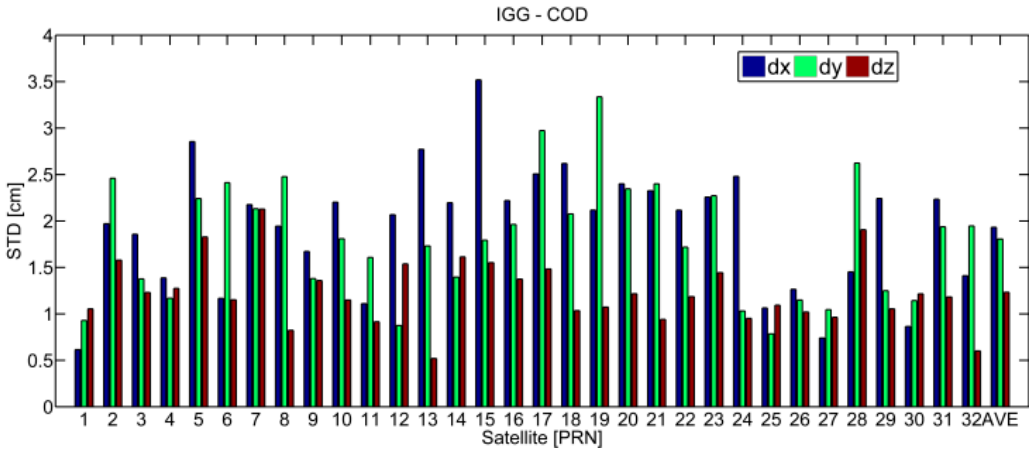

Figure 11. Standard deviation (STD) values using the three-step method for 25 August 2017.

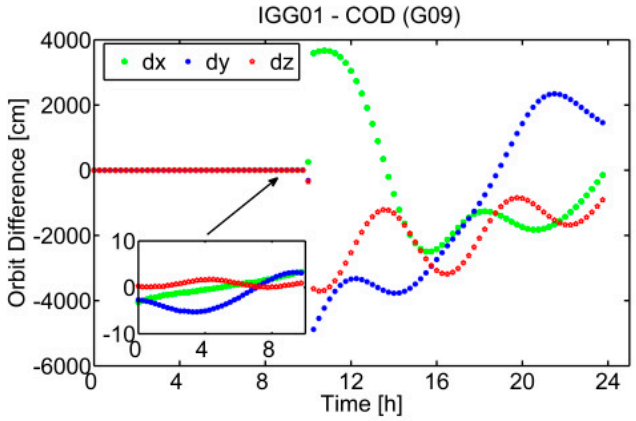

Figure 12. G09 orbit difference between IGG01 and COD for 25 August 2017.

Table 5. Orbital differences statistical results for satellite G09.

G09	RMS (cm)			STD (cm)			Radial (cm)	
	dx	dy	dz	dx	dy	dz	RMS	STD
IGG-COD	1.7	1.3	1.3	1.6	1.3	1.3	1.31	1.22
IGG01-COD	1534.0	2071.5	1639.7	1520.8	1953.0	1183.8	1487.31	1417.64

As seen in Figures 10–12 and Table 5, because the time of separate sub-arc of the IGG01 solution in POD was later than that of the IGG solution, the consistency between IGG orbits and CODE orbits was significantly improved compared to the consistency between IGG01 orbits and CODE orbits.

2. POD test based on data for 14 September 2017. The computed orbits (IGG) were compared with the CODE orbits in the X, Y, and Z directions. The RMS and STD values for the difference between orbits are shown in Figures 13 and 14, respectively.

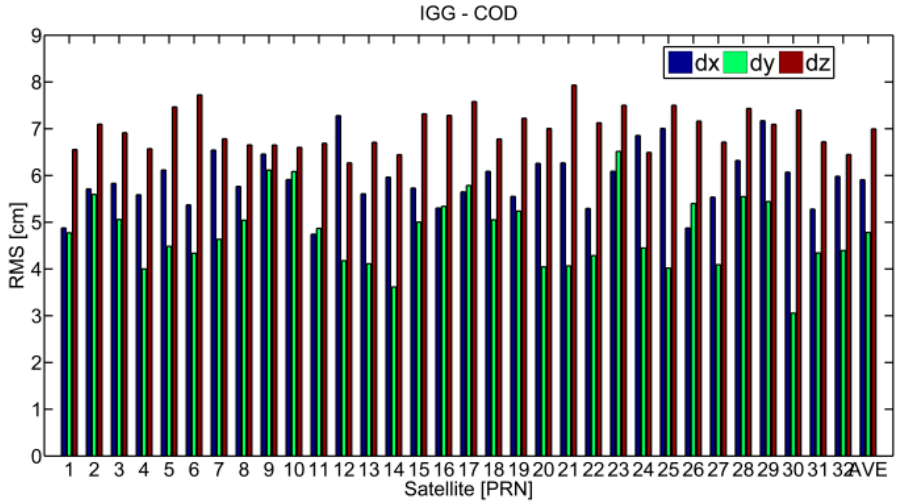

Figure 13. RMS values using the three-step method for 14 September 2017.

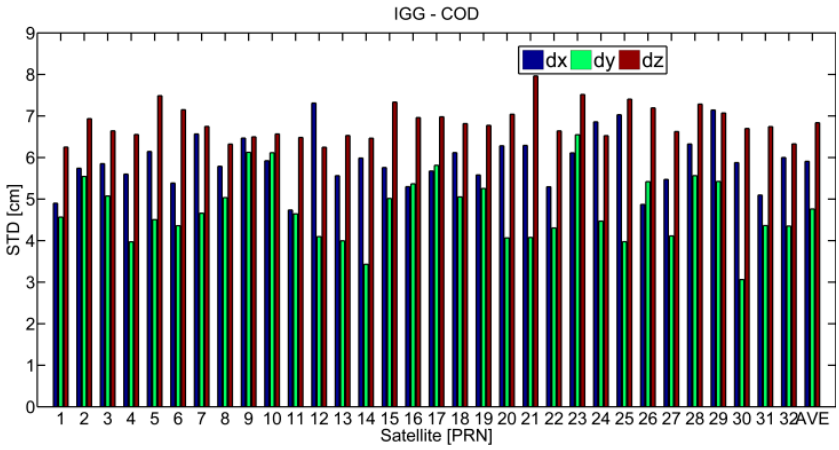

Figure 14. STD values using the three-step method for 14 September 2017.

4. Discussion

As seen in Figures 2–4 and Table 2, all four validations and traditional methods showed that G09 was abnormal on 25 August 2017, suggesting that there was an orbit leap of satellite G09 in the broadcast ephemeris on that date. Comparing each time period of the five verification methods, the broadcast ephemeris and information from NAVCEN provided a greater time range than other verification methods, which resulted in about a 2-hour reduction in observation utilization for G09. Furthermore, the unhealthy start-time using the three-step method was similar to the time provided by CODE's satellite crux files, and the unhealthy end-time from the proposed method was closer to the time provided by NAVCEN. Compared to the traditional method, the unhealthy start-time using the three-step method was closer to that provided by CODE.

As seen in Figures 5–7 and Table 3, the results from the three-step method showed that G01 of the broadcast ephemeris had an unhealthy time period. CODE's satellite crux files showed that G01 was in a healthy state, while the information from NAVCEN and the traditional method showed an unhealthy time period. The traditional method misjudged the orbit status of G01. In fact, there was not an orbit leap of G01 on 14 September 2017. Furthermore, as seen in Figures 5 and 7, the synchronized pseudo-range residuals of the traditional method were susceptible to abnormal values when eliminating the clock offset, and this result was also consistent with the disadvantages of the traditional method. From the broadcast ephemeris, the ephemeris data of G01 were missing at UTC 01:59:42–07:59:10. However, in normal circumstances, the ephemeris data of G01 should have been updated at GPST 04:00:00 and 06:00:00. As seen in Figure 8, we know that the available number of

observations from G01 was almost zero at GPST 00:20:30–06:14:30. Therefore, the signal transmission status of G01 was abnormal at GPST 00:20:30–06:14:30.

Figures 10 and 11 reveal that using unhealthy time period information detected by the three-step method resulted in RMS and STD values <2 cm for the difference between the computed orbit (IGG) and the orbit from CODE in the X, Y, and Z directions. In contrast, as seen in Figure 12 and Table 5, using the traditional method resulted in the RMS and STD values >10 m for the difference between the computed orbit (IGG01) and orbit from CODE in the X, Y, and Z directions.

As shown in Figures 13 and 14, the orbit from satellite G01 on 14 September 2017 did not need to be split into two arcs to determine the orbit. Besides, like other satellites, the accuracies between the IGG and CODE orbital solutions were of the same order of magnitude. In contrast, the traditional method misjudged the satellite orbit state of the broadcast ephemeris.

In general, the proposed method allowed a single-epoch solution, and it could detect the unhealthy orbit arc of the broadcast ephemeris in each theoretical observation sampling. Furthermore, the run-time of the proposed method was much less than one second in the detection of each sampling and the tests could be considered as real-time simulations. Compared to the traditional method, unhealthy orbit arc detection of the proposed method could be implemented simultaneously in multiple threads, and the characteristic could be used to detect unhealthy orbit arcs of broadcast ephemerides all day long. Since the robust method was added to the implementation of this proposed method, the three-step method was rather robust when eliminating the clock offset and judging the unhealthy time period. According to the unhealthy orbit information of the broadcast ephemeris detected by this proposed method, it can meet the requirements of GPS satellite POD when the broadcasting ephemeris is used as the initial orbit source. On the other hand, it can provide feasible information in the process of generating ultra-rapid/real-time orbits rather than waiting for updates of CODE's satellite crux files or for accumulating delayed observation data.

As mentioned above, the tests are theoretical simulations in real-time. There are other problems in processing real-time data streams, and the ability to provide stable reliable unhealthy orbit information in real-time requires further testing. Furthermore, the three-step method will be further used to analyze the ability to detect unhealthy orbit information of broadcast ephemerides of the BDS, Galileo, GLONASS, and other navigation systems.

5. Conclusions

In view of the fact that the current level of unhealthy orbit information of broadcast ephemerides cannot fully meet the requirements for rapid and real-time geodetic applications, especially when the broadcast ephemeris is used to create an a priori orbit during POD, we proposed a three-step method. Subsequently, the performance of the proposed three-step method was evaluated using the data from the IGS network for G09 and G01 satellites. A cross-validation was performed to compare the results from the three-step method and information provided by the CODE, NAVCEN, broadcast ephemeris, and the traditional method. From the two aspects of theory and results of cross-validation, for the proposed three-step method, we can conclude that:

1. It can provide a feasible approach to detect unhealthy time periods of satellite orbits of broadcast ephemerides in real-time.
2. It allows unhealthy time period detection for a satellite orbit of a broadcast ephemeris all day long by comprehensive evaluation.
3. Compared to the unhealthy orbit arc information of NAVCEN and the broadcast ephemeris, the proposed method can increase observation utilization of an unhealthy satellite of about several hours.
4. Compared to the traditional method, the proposed method helps to improve the reliability of unhealthy orbit arc information. Firstly, the unhealthy start-time of the satellite orbit of the broadcast ephemeris, using the three-step method, is closer to that provided by CODE. Secondly, the traditional method can misjudge the orbit status of a satellite of the broadcast ephemeris. In

contrast, the proposed three-step method can distinguish the orbit status of a satellite. Besides, the traditional method is susceptible to abnormal values when eliminating the clock offset, and this result is also consistent with the theory. Last but not least, in the POD application, using the unhealthy time period detected by the three-step method shows an improvement in orbit accuracy.

Author Contributions: F.Y., Y.Y., and B.Z. provided the initial idea for this study; F.Y., Y.Y., and B.Z. conceived and designed the analysis; F.Y., Y.Y., B.T., B.Z., and J.O. analyzed the results; F.Y., Y.Y., B.Z., and B.T. wrote the paper.

Funding: This work was supported by the Collaborative Precision Positioning Project funded by the Ministry of Science and Technology of China (No. 2016YFB0501900) and China Natural Science Funds (No. 41604033, 41574015, 41574033).

Acknowledgments: The authors also acknowledge the LU JIAXI International team program supported by the K.C. Wong Education Foundation and CAS. The authors would like to thank the IGS network for providing the GPS data. Thanks to Qingsong Ai and Ying Li for their help in modifying this article.

Conflicts of Interest: The authors declare no conflict of interest.

References

1. Lichten, S.M.; Border, J.S. Strategies for high-precision Global Positioning System orbit determination. *J. Geophys. Res. Solid Earth* **1987**, *92*, 12751–12762. [CrossRef]
2. Montenbruck, O.; Schmid, R.; Mercier, F.; Steigenberger, P.; Noll, C.; Fatkulin, R.; Kogure, S.; Ganeshan, A.S. GNSS satellite geometry and attitude models. *Adv. Space Res.* **2015**, *56*, 1015–1029. [CrossRef]
3. Montenbruck, O.; Steigenberger, P.; Prange, L.; Deng, Z.G.; Zhao, Q.L.; Perosanz, F.; Romero, I.; Noll, C.; Sturze, A.; Weber, G.; et al. The Multi-GNSS Experiment (MGEX) of the International GNSS Service (IGS)—Achievements, prospects and challenges. *Adv. Space Res.* **2017**, *59*, 1671–1697. [CrossRef]
4. Guo, J.; Chen, G.; Zhao, Q.; Liu, J.; Liu, X. Comparison of solar radiation pressure models for BDS IGSO and MEO satellites with emphasis on improving orbit quality. *GPS Solut.* **2017**, *21*, 511–522. [CrossRef]
5. Zhao, Q.; Chen, G.; Guo, J.; Liu, J.; Liu, X. An a priori solar radiation pressure model for the QZSS Michibiki satellite. *J. Geod.* **2018**, *92*, 109–121. [CrossRef]
6. Li, X.; Chen, X.; Ge, M.; Schuh, H. Improving multi-GNSS ultra-rapid orbit determination for real-time precise point positioning. *J. Geod.* **2018**. [CrossRef]
7. Kang, Z.; Tapley, B.; Bettadpur, S.; Ries, J.; Nagel, P.; Pastor, R. Precise orbit determination for the GRACE mission using only GPS data. *J. Geod.* **2006**, *80*, 322–331. [CrossRef]
8. Kusche, J. Approximate decorrelation and non-isotropic smoothing of time-variable GRACE-type gravity field models. *J. Geod.* **2007**, *81*, 733–749. [CrossRef]
9. Jäggi, A.; Hugentobler, U.; Bock, H.; Beutler, G. Precise orbit determination for GRACE using undifferenced or doubly differenced GPS data. *Adv. Space Res.* **2007**, *39*, 1612–1619. [CrossRef]
10. Li, X.; Ge, M.; Dai, X.; Ren, X.; Fritsche, M.; Wickert, J.; Schuh, H. Accuracy and reliability of multi-GNSS real-time precise positioning: GPS, GLONASS, BeiDou, and Galileo. *J. Geod.* **2015**, *89*, 607–635. [CrossRef]
11. Guo, F.; Li, X.; Zhang, X.; Wang, J. Assessment of precise orbit and clock products for Galileo, BeiDou, and QZSS from IGS Multi-GNSS Experiment (MGEX). *GPS Solut.* **2017**, *21*, 279–290. [CrossRef]
12. Kazmierski, K.; Sosnica, K.; Hadas, T. Quality assessment of multi-GNSS orbits and clocks for real-time precise point positioning. *GPS Solut.* **2017**, *22*, 12. [CrossRef]
13. Dach, R.; Lutz, S.; Walser, P.; Fridez, P. *Prepare the Orbit Improvement. Bernese GNSS Software Version 5.2*; Astronomical Institute, University of Bern: Bern, Switzerland, 2015; p. 379.
14. He, L.; Ge, M.; Wang, J.; Wickert, J.; Schuh, H. Experimental study on the precise orbit determination of the BeiDou navigation satellite system. *Sensors* **2013**, *13*, 2911–2928. [CrossRef]
15. Ye, F.; Yuan, Y.; Ou, J. Initial orbit determination of BDS-3 satellites based on new code signals. *Geod. Geodyn.* **2018**, *9*, 342–346. [CrossRef]
16. Heng, L.; Gao, G.X.; Walter, T.; Enge, P. GPS ephemeris error screening and results for 2006–2009. In Proceedings of the 2010 International Technical Meeting of the Institute of Navigation (ION ITM 2010), San Diego, CA, USA, 25–27 January 2010; pp. 1014–1022.
17. Wang, H.; Jiang, H.; Ou, J.; Sun, B.; Zhong, S.; Song, M.; Guo, A. Anomaly analysis of 18 years of newly merged GPS ephemeris from four IGS data centers. *GPS Solut.* **2018**, *22*, 124. [CrossRef]

18. Steigenberger, P.; Hugentobler, U.; Hauschild, A.; Montenbruck, O. Orbit and clock analysis of Compass GEO and IGSO satellites. *J. Geod.* **2013**, *87*, 515–525. [CrossRef]
19. Byun, S. Satellite orbit determination using triple-differenced GPS carrier phase in pure kinematic mode. *J. Geod.* **2003**, *76*, 569–585. [CrossRef]
20. Huang, Y.; Hu, X.; Zhang, X.; Jiang, D.; Guo, R.; Wang, H.; Shi, S. Improvement of orbit determination for geostationary satellites with VLBI tracking. *Chin. Sci. Bull.* **2011**, *56*, 2765. [CrossRef]
21. Cao, F.; Yang, X.; Li, Z.; Sun, B.; Kong, Y.; Chen, L.; Feng, C. Orbit determination and prediction of GEO satellite of BeiDou during repositioning maneuver. *Adv. Space Res.* **2014**, *54*, 1828–1837. [CrossRef]
22. Davis, T.; Melanson, D. XSS-10 microsatellite flight demonstration program results. *Spacecr. Platf. Infrastruct.* **2004**, *5419*, 16–26.
23. Ye, F.; Yuan, Y.; Tan, B.; Ou, J. A robust method to detect beidou navigation satellite system orbit maneuvering/anomalies and its applications to precise orbit determination. *Sensors* **2017**, *17*, 1129. [CrossRef] [PubMed]
24. Liu, Z.; Qu, L.; Zhao, Q. Real -time Anomaly Detection of BDS Broadcast Ephemeris. In Proceedings of the Fifth China Satellite Navigation Conference (CSNC), Nanjing, China, 21–23 May 2014; pp. 107–112.
25. Huang, G.; Qin, Z.; Zhang, Q.; Wang, L.; Yan, X.; Fan, L.; Wang, X. A real-time robust method to detect BeiDou GEO/IGSO orbital maneuvers. *Sensors* **2017**, *17*, 2761. [CrossRef] [PubMed]
26. Huang, G.; Qin, Z.; Zhang, Q.; Wang, L.; Yan, X.; Wang, X. An optimized method to detect BDS satellites' orbit maneuvering and anomalies in real-time. *Sensors* **2018**, *18*, 726. [CrossRef] [PubMed]
27. Dow, J.M.; Neilan, R.E.; Rizos, C. The international GNSS service in a changing landscape of global navigation satellite systems. *J. Geod.* **2009**, *83*, 191–198. [CrossRef]
28. Hugentobler, U.; Meindl, M.; Beutler, G.; Bock, H.; Dach, R.; Jäggi, A.; Urschl, C.; Mervart, L.; Rothacher, M.; Schaer, S. *CODE IGS Analysis Center Technical Report 2003/2004*; Gowey, K., Neilan, R., Moore, A., Eds.; IGS 2004 Technical Reports; IGS Central Bureau: Bern, Switzerland, 2006.
29. Dach, R.; Lutz, S.; Walser, P.; Fridez, P. The Osculating Orbital Elements/Checking GNSS Broadcast Messages. In *Bernese GNSS Software Version 5.2*; Astronomical Institute, University of Bern: Bern, Switzerland, 2015; pp. 32–46, 107–125.
30. Tsai, Y.-J. Wide area Differential Operation of the Global Positioning System: Ephemeris and Clock Algorithms. Ph.D. Dissertation, Stanford University, Stanford, CA, USA, 1999.
31. Kee, C.; Parkinson, B.W.; Axelrad, P. Wide area differential GPS. *Navigation* **1991**, *38*, 123–145. [CrossRef]
32. Hwang, P.Y.; McGraw, G.A.; Bader, J.R. Enhanced differential GPS carrier-smoothed code processing using dual-frequency measurements. *Navigation* **1999**, *46*, 127–137. [CrossRef]
33. Rothacher, M.; Springer, T.; Schaer, S.; Beutler, G. Processing strategies for regional GPS networks. In *Advances in Positioning and Reference Frames*; Springer: Berlin/Heidelberg, Germany, 1998; pp. 93–100.
34. Yan, W.; Ou, J.; Yuan, Y.; Salazar, D. Research on network augmented real-time precise point positioning algorithm with broadcast ephemeris. *Geomat. Inf. Sci. Wuhan Univ.* **2012**, *37*, 1190–1193. [CrossRef]
35. Montenbruck, O.; Steigenberger, P.; Hauschild, A. Broadcast versus precise ephemerides: A multi-GNSS perspective. *GPS Solut.* **2015**, *19*, 321–333. [CrossRef]
36. Yang, Y. Robust estimation of geodetic datum transformation. *J. Geod.* **1999**, *73*, 268–274. [CrossRef]
37. Boehm, J.; Heinkelmann, R.; Schuh, H. Short Note: A global model of pressure and temperature for geodetic applications. *J. Geod.* **2007**, *81*, 679–683. [CrossRef]
38. Boehm, J.; Niell, A.; Tregoning, P.; Schuh, H. Global Mapping Function (GMF): A new empirical mapping function based on numerical weather model data. *Geophys. Res. Lett.* **2006**, *33*, 4. [CrossRef]